Carbon-Embedded Nodal Energy Price in Hydrogen-Blended Integrated Electricity and Gas Systems With Heterogeneous Gas Compositions

Sheng Wang, *Member, IEEE,* Hongxun Hui, *Member, IEEE,* Junyi Zhai, *Member, IEEE,* Pierluigi Siano, *Senior Member, IEEE*

Abstract—Blending green hydrogen from renewable generations into the natural gas infrastructure can effectively mitigate carbon emissions of energy consumers. However, distributed hydrogen blending could lead to heterogeneous gas compositions across the network. The traditional nodal energy price scheme is designed for uniform gas composition, which cannot reflect the impacts of heterogeneous nodal gas composition and carbon emission mitigation. This paper proposes a novel nodal energy price scheme in hydrogen-blended integrated electricity and gas systems (H-IEGS). First, we propose a joint market-clearing model for H-IEGS, where the nonlinear physical properties of gas mixtures caused by heterogeneous gas compositions are characterized. The impacts of hydrogen blending on the carbon emission cost are also quantified. To retrieve the nodal energy price from this highly nonlinear and nonconvex optimization problem, a successive second-order cone programming (SSOCP) method is tailored to get the dual variables tractably. Considering the continuous market clearing process, a warm-start technique is proposed to provide initial reference points for the SSOCP to improve computation efficiency. Finally, an H-IEGS test case in Belgium and a large-scale practical case in Northwest China are used to validate the effectiveness of the proposed method.

Index Terms—nodal energy price, hydrogen, integrated electricity and gas systems, gas composition, carbon emission

NOMENCLATURE

A. Indices, sets, and functions

δ	Matrix of slack variables
λ, ν, ω	Matrices of dual variables
φ	Matrix of penalty factors
$A, ..., F, P, Q$	Matrices of coefficients in the optimization problem
g	Matrix of electricity generation
p, q	Matrices of gas pressure and gag flow
u, x	Matrices of control and state variables
ι	Index for iteration
$\mathcal{I}, \mathcal{J}$	Sets for bus

$h, \mathcal{H}$	Index and set for power-to-gas
i, j	Indices for bus
$k, \mathcal{K}$	Index and set for dispatch interval
l, L	Index and set for generator
$m, \mathcal{M}$	Index and set for constraint
$n, \mathcal{N}$	Index and set for gas component
$s, \mathcal{S}$	Index and set for gas source

B. Variables

$\chi_{i,k,n}, \chi_{ij,k,n}$	Fraction of gas component n at a gas bus or in a pipeline
$\lambda^e_{i,k}, \lambda^g_{i,k,n}$	Nodal electricity/gas price for gas component n (\$/MWh, \$/Nm^3)
$\psi_{ij,k}$	linepack energy (J)
$\rho_{i,k}, \rho_{ij,k}$	Gas density of the gas mixture at a gas bus or in a pipeline (kg/Nm^3)
$\theta_{i,k}$	Voltage angle
$g^{ptg}_{i,h,k}$	Electricity consumption of power-to-gas (MW)
$g^{tpp}_{i,l,k}$	Electricity generation of traditional non-gas-fired power plant (MW)
$g_{ij,k}$	Electricity power flow on a electric branch (MW)
$p_{i,k}$	Gas pressure (bar)
$q^{me}_{i,h,k}, q^{hy}_{i,h,k}$	Methane/hydrogen production of power-to-gas (Nm^3/day)
$q^{ptg}_{i,h,k}, q^{ptg}_{i,h,k,n}$	Gas production of power-to-gas for (gas component n) (Nm^3/day)
$q^d_{i,k}, q^d_{i,k,n}$	Gas demand of (gas component n) (Nm^3/day)
$q^{gpp}_{i,l,k,n}$	Gas consumption of gas component n of gas-fired power plant (Nm^3/day)
$q^{gs}_{i,s,k}, q^{gs}_{i,s,k,n}$	gas production of (gas component n) of gas source (Nm^3/day)
$q_{ij,k}, q_{ij,k,n}$	Gas flow in the pipeline for (gas component n) (Nm^3/day)
$RD_{i,k}$	Relative density (kg/Nm^3)
$r_{ij,k}$	Gas constant of the gas mixture (J/(mol·K))
$WI_{i,k}, FS_{i,k}$	Wobbe index (J/Nm^3) and flame speed factor

C. Parameters

$(\cdot)^{min}, (\cdot)^{max}$	Lower and upper bounds for variable $(\cdot)$
α_{ij}	Linepack energy threshold
$\beta^{gs}_{i,s}, \beta^{tpp}_{i,l}, \beta^{ptg}_{i,h}$	Carbon emission coefficients of gas source and transitional non-gas-fired power plant (kg/Nm^3)
$\chi^{ni}_{i,k}, \chi^{ox}_{i,k}$	Fractions of nitrogen and oxygen
$\chi^{gs}_{i,s,n}$	Gas composition of gas source
$\eta^{gpp}_{i,l}, \eta^{el}_{i,h}, \eta^{me}_{i,h}$	Efficiencies of gas-fired power plant, electrolysis, and methanation processes
γ_{ij}	Gas flow direction

This article has been accepted for publication in IEEE Transactions on Sustainable Energy. This is the author's version which has not been fully edited and content may change prior to final publication. Citation information: DOI 10.1109/TSTE.2024.3372628

2

μ^{cd}	Subsidy for carbon dioxide capture (\$/Nm^3)
$\mu_{i,s}^{gs}$	Gas production cost of gas source (\$/Nm^3)
$\rho^{cd,stp}, \rho^{ng,stp}$	Gas density of carbon dioxide/natural gas in standard temperature and pressure condition (kg/Nm^3)
Θ_{ij}	Property coefficient of the pipeline
ϑ	Multiplier for penalty factor
$a_{i,l}, b_{i,l}$	Generation cost coefficients (\$/MW^2, \$/MW)
AF	Air-fuel ratio
C_n	Numbers of carbon atom in the molecule of gas component n
f_{ij}, L_{ij}, D_{ij}	Friction factor, length (m), and diameter of pipeline (m)
fs_n	Flame speed factor
GCV_n	Gross calorific value (J/Nm^3)
M_n, M^{air}	Molecular weights of gas component n and air (kg/Nm^3)
$q_{i,k}^{d,ng}$	Gas demand measured with original natural gas (Nm^3)
R_n	Gas constant
T^{ng}, Z^{ng}	Temperature (K) and compressibility factor of natural gas
V_{ij}	Volume of the pipeline (m^3)
X_{ij}	Reactance (Ω)

I. Introduction

BLENDING green gases (such as hydrogen) from renewable generations into the existing gas infrastructures are expected to play an important role in facilitating the transition towards a net-zero energy system. With a larger fraction of hydrogen in the gas, the same energy demand of consumers can be satisfied with less carbon dioxide emissions. Many countries have published policies or conducted small-scale trials to explore the feasibility of hydrogen blending, As shown in Table. I, most of the hydrogen blending projects are carried out at the distributional level, and a recently published strategic policy decision by the UK on Dec 2023 has approved its feasibility [1]. The transmission-level hydrogen blending is under trial and evidence collecting, e.g., HyNet and FutureGrid, but is still very promising in the near future due to its great potential for decarbonization. It can be estimated that more than 6 Mt of equivalent carbon dioxide emission can be avoided if the current natural gas system is blended with 20% hydrogen [2]. Together with the increasing adoption of gas-fired power plants, hydrogen integration via power-to-gas (PTG) plants further facilitates the integration of electricity and gas systems. Thus, the concept of hydrogen-blended integrated electricity and gas systems (H-IEGS) is developed.

Nonetheless, hydrogen blending in the H-IEGS poses great challenges to the current nodal energy price scheme, which has been reported by the Energy Network Association, etc. [18]. The existing nodal energy price scheme assumes the transmission of a relatively homogeneous natural gas. With distributed hydrogen injections, gas compositions at different locations become inconsistent. For example, as shown in Fig. 1, due to hydrogen's lower gross caloric value (GCV), the GCV of the gas mixture at gas bus 2 is lower than at gas
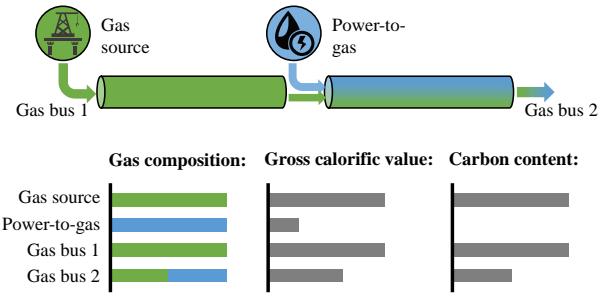

Fig. 1. Illustration of nodal energy prices in gas systems with heterogeneous gas compositions (green and blue colors represent natural gas and hydrogen respectively).

bus 1. Consequently, the gas appliance of consumers cannot produce the same energy by consuming the same volume of gas. Therefore, it is unfair to charge gas consumers at different locations based on the traditional nodal energy price scheme regardless of the differences in GCVs. Moreover, the heterogeneous gas composition also results in inconsistent carbon contents in gas mixtures. For example, as shown in Fig. 1, since there is no carbon element in hydrogen, the carbon content of the gas mixture at gas bus 2 is lower than at gas bus 1. With various forms of carbon-emission-related costs (such as carbon emission budget/tax/penalty, etc.) coming up to the stage, the value of hydrogen blending in reducing external carbon-emission costs should also be quantified in the energy market clearing. Therefore, it is essential to develop a new pricing methodology in the electricity and gas market, which can effectively reflect the impacts of heterogeneous gas compositions.

Though the nodal electricity price scheme in competitive markets has been extensively studied in the past decades [19]–[21], its applications in integrated energy systems are at an early stage. For example, the basic mathematical forms of marginal nodal electricity, gas, and heat prices in integrated energy systems are proposed in [22]. It is further embedded with potential carbon emission cost in [23]. The market equilibrium of electricity and gas prices based on bilateral trading is proposed in [24]. A generalized marginal price scheme and its decomposition method in integrated electricity-gas-heat systems are proposed in [25]. Nodal energy prices are used for optimal operation and strategic bidding in [26] and [27], respectively. Recently, a few studies have extended the nodal energy price scheme to energy systems with the participation of hydrogen. For example, the marginal energy pricing scheme for hydrogen is proposed in [28]. It is also integrated with power and transportation systems to guide the refueling of fuel cell vehicles in [29]. However, all these studies aim at the nodal energy price of homogeneous gas systems (pure natural gas or pure hydrogen), which cannot reflect the impacts of heterogeneous gas compositions as aforementioned.

The prerequisite for establishing the nodal energy price scheme in H-IEGS with heterogeneous gas compositions is to develop an accurate market clearing model with practical physical constraints. The heterogeneous gas compositions variablize the physical properties of gas mixtures (such as specific gravity) that used to be constant in homogeneous

This article has been accepted for publication in IEEE Transactions on Sustainable Energy. This is the author's version which has not been fully edited and content may change prior to final publication. Citation information: DOI 10.1109/TSTE.2024.3372628

3

TABLE I
HYDROGEN BLENDING POLICIES AND PROJECTS IN THE MAJOR COUNTIES/REGIONS TODAY

	Policy papers	Demonstration Projects
Europe	· EU hydrogen policy (Jul 2020) [3]: 5-10% hydrogen injection in the immediate future. · UK hydrogen strategy (Aug 2021) [4]: 20% hydrogen by late 2022. · The National Hydrogen Strategy (Germany, Jun 2020) [5]: hydrogen blending (up to 10%) at the distribution level.	· NaturalHy (EU, 2004 - 2009) [6]: 20% in the distribution system. · GRHYD (France, 2014) [7]:, 6%-20% in transportation sector. · SNAM (Italy, 2021) [8]: 30% hydrogen in steel-forging. · HyDeploy (the UK, 2019-now) [9]: 20% blending for University and residential users. · HyNet (the UK, 2025) [10]: largest hydrogen blending test. · FutureGrid (the UK, 2021) [11]: high-pressure hydrogen blending test.
The US	· US National Clean Hydrogen Strategy and Roadmap (Jun 2023) [12]: 1-3 MMT/year hydrogen blending demand in 2050.	· HyBlend (2021-2023) [2]: evaluate the imapct of hydrogen blending for up tp 30%.
China	· Opinions on Improving the System, Mechanism, and Policy Measures for Energy Green and Low-Carbon Transformation, Medium, and long-term plan for the development of the hydrogen energy industry (2021-2035) (Mar 2022): suggest carrying out the reliability, cost-benefit, adaptability, and integrity analysis of hydrogen blending pipelines and other key equipment.	· Chaoyang (2019) [13]: operates safely with 10% hydrogen for one year. · Zhangjiakou (2020) [14]: hydrogen-blended with 4 Mm^3/year hydrogen capacity. · Zhanjiang (2021) [15]: first hydrogen blending pipeline under the sea.
Others	· Australia's National Hydrogen Strategy (Nov 2019): regards the blending of hydrogen as a strategic focus area, but will not support transmission network blending until hydrogen embrittlement issues can be safely addressed [16].	· Hyp SA (Australia, 2021) [17]: 5% green hydrogen for Adelaide.

gas systems. It greatly affects the energy flow pattern in H-IEGS, increasing the complexity of the whole optimization problem. Recently, a few studies have begun to focus on constructing the optimal energy flow problem in H-IEGS. An integrated optimization framework in H-IEGS is first proposed in [30]. It is further extended to robust optimization with wind fluctuation [31], volt-VAR-pressure regulation [32], and flexibility region quantification of PTGs [33]. The long-term and short-term impacts of alternative gas injection on reliability are comprehensively studied in [34], [35]. However, these studies cannot be used directly in market clearing. On the one hand, detailed physical constraints (such as the impacts of gas composition variations on the specific gravity in gas flows) are usually overlooked to simplify the calculation. As a result, the optimization results cannot accurately reflect the impacts of hydrogen blending on the nodal energy price. On the other hand, some optimization models are still nonconvex and are solved with general nonlinear solvers. The dual problem can not be tractably obtained to calculate the nodal energy price.

To address the research gaps, this paper proposes a novel nodal energy price scheme in the carbon emission-embedded H-IEGS considering heterogeneous gas compositions. The detailed contributions are summarized as follows:

1) A novel joint market clearing model for H-IEGS is proposed, where: i) The detailed physical constraints on gas flow considering the impact of gas composition variations are incorporated to improve the accuracy of the optimization model. ii) Carbon emission cost is also leveraged to reflect the values of hydrogen blending in carbon emission reductions. iii) Linepack energy is restrained to maintain the robustness of the H-IEGS during continuous market operation. Compared to the traditional nodal energy price scheme, the proposed scheme can guarantee fairness for energy consumers by considering spatial differences in gas compositions.

2) A tractable solution method for nodal energy prices in H-IEGS is proposed, where: i) Taylor approximation is tailored to tackle the high nonlinearities and non-convexities with different forms in the market clearing problem. ii) A successive second-order cone program-

ming (SSOCP) is developed. It uses convex optimization models and adaptively increasing penalty factors to gradually approximate the original model, so that the dual problem can be formulated to obtain the nodal energy price. iii) A warm-start technique is developed to provide initial reference points for SSOCP based on historical operation data, so the computation efficiency can be improved during the continuous market clearing.

3) The effects of the proposed nodal energy price scheme are comprehensively investigated using practical large-scale Northwest H-IEGS in China. By considering the heterogeneous gas composition and carbon emission, the average nodal gas price decreased by 8.48% lower than the value without hydrogen injection. It shows that our scheme can both reflect the impacts of the inconsistent GCV and values of decarbonization by the hydrogen injection, which could provide more incentives in future market operations. Moreover, the major constraints from gas quality on the nodal energy price are identified through sensitivity analysis. If the gas security constraints are further relaxed due to technical advancement, the nodal energy price can decrease by 9%, which further reveals the value of hydrogen blending in the energy system decarbonization.

II. ILLUSTRATION OF NODAL ENERGY PRICE IN H-IEGS

The structure of the H-IEGS is shown in Fig. 2. (a). The H-IEGS contains two networks, namely, the electricity network and the gas network. The electricity is mainly supplied by traditional fossil power plants (which use fossil fuels other than gas to generate electricity) and renewable generation (mainly refer to wind farms in this paper). The gas system is mainly supplied by natural gas and biogas sources. Gas-fired power plants and PTG are the key components that couple the two energy systems. Gas-fired power plants consume gas from the gas system to generate electricity, while PTGs produce hydrogen and methane by consuming surplus renewable generations. The alternative gas injection process is shown in Fig. 1. The hydrogen can be further injected into the gas pipelines
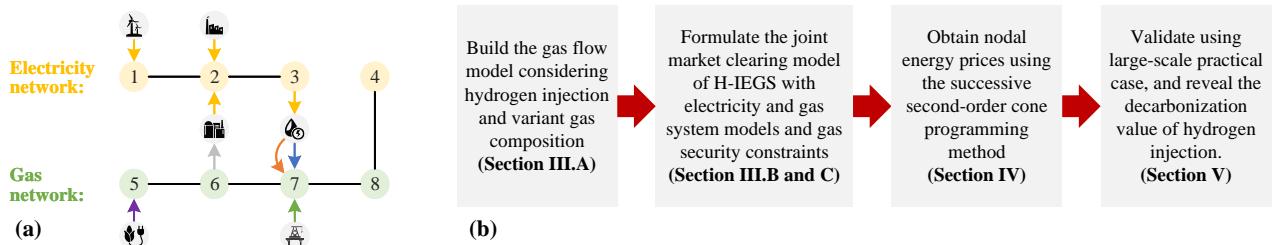
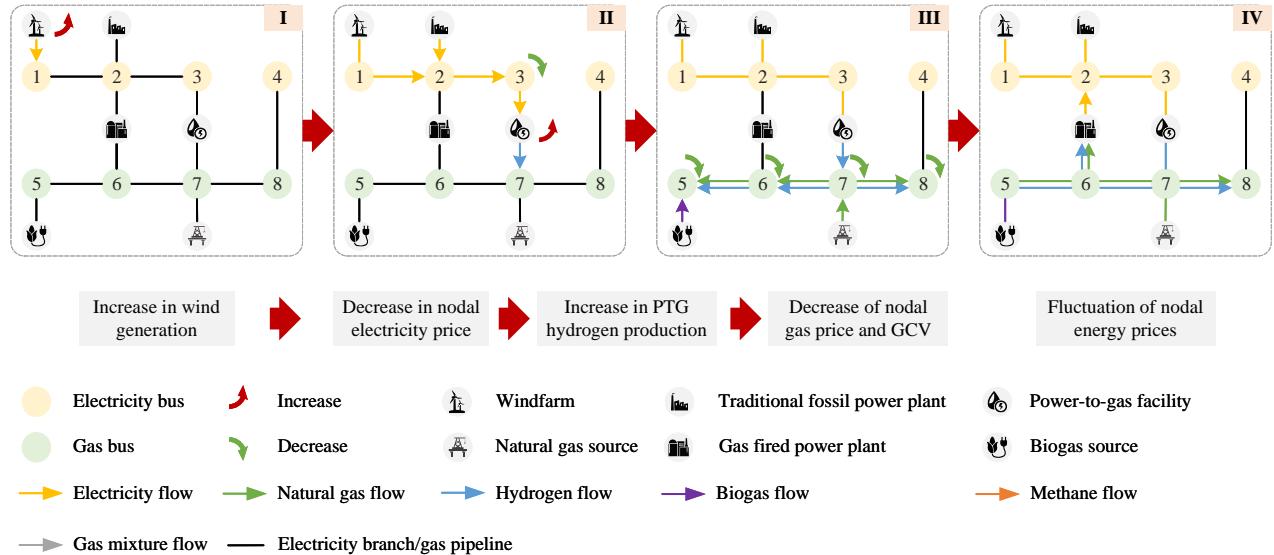Fig. 2.   (a) Structure of H-IEGS; (b) general flow chart.

Fig. 3.   Illustration of nodal energy price coupling.

and fully mixed. Then, the gas mixture will be transported to other locations to meet the demands of energy consumers.

Fig. 3 shows how renewable generation and hydrogen blending affect both nodal electricity and gas prices. Generally in energy systems, nodal energy prices are affected by many factors, such as renewable generations, load levels, etc. Particularly in H-IEGS, the nodal energy prices in two energy systems are affected by the hydrogen blending modes, and are tightly coupled by gas-fired power plants and PTGs. For example, as shown in Fig. 3, the propagation of nodal energy prices can be illustrated by four phases. In phase I, we assume that the wind power increases. Then in phase II, due to the lower marginal price of wind generation, the electricity buses that are close to the wind farms (e.g., #1, #2, and #3) will have lower nodal electricity prices. Then, the hydrogen production of PTG at electricity bus #3 may increase (suppose the gas security limits are not violated). In phase III, because the hydrogen fraction in the injection point (gas bus #7) is higher, the GCV and nodal gas price will decrease. This hydrogen content will also propagate to adjacent gas buses (such as #5, #6, and #8), causing their GCV and nodal price to decrease. In Phase IV, the joint effects of lower GCV and lower gas cost may further affect the generation cost of gas-fired power plants, and thus influence the electricity prices in return.

To investigate this problem, this paper is implemented mainly in four steps, as shown in Fig. 2. (b). The analysis of the nodal energy price scheme includes three major steps,

which are depicted in Sections III and IV. Section III.A focus on building the gas flow model considering the hydrogen injections and consequent variant gas compositions. Then, by considering the coupling in two energy systems and gas security constraints, we formulate the joint market-clearing model. In Section IV, the original nonconvex optimization problem is reformulated into a tractable second-order-cone programming problem, and then solved using successive programming methods to obtain the nodal energy price. Finally, in the case study, small and large-scale cases are both used to demonstrate the superiority of our price scheme, which can reflect the impacts and decarbonization value of hydrogen injection.

III. Joint Market Clearing Model of H-IEGS

The nodal energy prices are obtained by the joint market clearing of H-IEGS in the day ahead based on the forecast wind speed and energy demands. The objective is to minimize the total operating cost of H-IEGS during the operation horizon, as shown in (1), including gas production cost, electricity generation cost, and carbon emission cost. Notably, the carbon dioxide emission can be penalized either on the supplied side or the demand side (as two widely adopted carbon calculation methods) [36]. In this work, we use the inventory-based method, and penalize the carbon dioxide emission that exceeds the carbon budget from the supply side. Since the electricity generation and gas supply will eventually be consumed by end-

This article has been accepted for publication in IEEE Transactions on Sustainable Energy. This is the author's version which has not been fully edited and content may change prior to final publication. Citation information: DOI 10.1109/TSTE.2024.3372628

5

users, we assume the complete combustion of gas, and thus it is equivalent to calculating carbon emissions from either the supply or demand side. The carbon emission includes the part from gas sources, traditional fossil power plants, and the carbon capture from PTGs (used as raw material to produce methane). Here we mainly focus on deterministic optimization, while it can be easily extended to stochastic and robust operation frameworks.

$$
\begin{aligned}
\min \sum_{k \in \mathcal{K}} \sum_{i \in \mathcal{I}} \Bigg(& \sum_{s \in \mathcal{S}_i} \left(\mu_{i,s}^{gs} q_{i,s,k}^{gs} + \mu^{cd} \beta_{i,s}^{gs} q_{i,s,k}^{gs} \right) \\
& + \sum_{l \in \mathcal{L}_i^{tpp}} \left(a_{i,l}(g_{i,l,k}^{tpp})^2 + b_{i,l} g_{i,l,k}^{tpp} + \mu^{cd} \beta_{i,l}^{tpp} g_{i,l,k}^{tpp} \right) \\
& - \sum_{h \in \mathcal{H}_i} \mu^{cd} \beta_{i,h}^{ptg} q_{i,h,k}^{me} \Bigg)
\end{aligned} \tag{1}
$$

where i and k are the indicators for the bus, dispatch interval, and system component, respectively; s, l, and h are indicators for gas source, generator, and PTG, respectively; $\mathcal{I}$ and $\mathcal{K}$ are the sets of buses and dispatch intervals, respectively; $\mathcal{S}_i$, $\mathcal{L}_i^{tpp}$, and $\mathcal{H}_i$ are the sets of gas sources, traditional fossil power plants, and PTGs at bus i, respectively; $q_{i,s,k}^{gs}$ is the gas production of gas source s at bus i in dispatch interval k; $g_{i,l,k}^{tpp}$ is the electricity generation of generator l at bus i in dispatch interval k; $q_{i,h,k}^{me}$ is the methane production of PTG h at bus i at dispatch interval k; $\beta_{i,s}^{gs}$ and $\beta_{i,l}^{tpp}$ are the carbon emission coefficients of gas source s and traditional fossil power plant l at bus i, respectively; they represent how much carbon dioxide will be produced by consuming unit gas supply or electricity supply from gas sources or generators; The calculation of these coefficients is introduced in (3). $\beta_{i,h}^{ptg}$ is the carbon capture coefficient of the methanation process of PTG h at bus i; It usually takes the value zero considering that the produced methane will be completely combusted eventually in the gas network. Some countries will offer subsidies to the electrolysis and methanation processes (such as in Jilin and Chengdu in China [37], [38]), and then it can also take corresponding values. $\mu_{i,s}^{gs}$ is the gas production price of gas source s at bus i; $a_{i,l}$ and $b_{i,l}$ are the coefficients of electricity generating cost of traditional fossil power plant l at bus i; μ^{cd} is the penalty price for carbon dioxide emission.

The joint market clearing problem is subject to physical constraints, as introduced in the following subsections.

A. Gas system constraints

Gases supplied from different gas sources have different gas compositions (e.g., the gas supply from biogas usually has a lower methane fraction than that from natural gas), as shown in (2). As a result, the carbon emission coefficients are different. We assume all the gases are combusted completely at the user's end. Then, the carbon emission factor can be calculated by (3). All the gas sources should operate within their upper and lower bounds as in (4).

$$
q_{i,s,k,n}^{gs} = \chi_{i,s,n}^{gs} q_{i,s,k}^{gs}, \ \sum_{n \in \mathcal{N}} \chi_{i,s,n}^{gs} = 1 \tag{2}
$$

$$
\beta_{i,s}^{gs} = \sum_{n \in \mathcal{N}} C_n \chi_{i,s,n}^{gs} \rho^{cd,stp} \tag{3}
$$

$$
q_{i,s}^{gs,min} \le q_{i,s,k}^{gs} \le q_{i,s}^{gs,max} \tag{4}
$$

where n is the index for gas composition; $\mathcal{N}$ is the set of gas compositions. In this paper, we consider seven typical components of natural gas, i.e., $n = 1, 2, ..., 7$, including methane, ethane, propane, butane, hydrogen, nitrogen, and carbon dioxide. $q_{i,s,k,n}^{gs}$ is the gas production of gas component n from gas source s at bus i in dispatch interval k; $\chi_{i,s,n}^{gs}$ is the molar fraction of gas component n of gas source s at bus i; C_n is the number of carbon atoms in gas component n; $\rho^{cd,stp}$ is the density of carbon dioxide in standard temperature and pressure conditions; $q_{i,s}^{gs,min}$ and $q_{i,s}^{gs,max}$ are the lower and upper bounds of gas source s at bus i, respectively.

The gas demand for gas appliances is usually combusted to produce heat energy, like gas water heaters, gas cooktops, etc. In the H-IEGS which has a lower GCV due to the hydrogen, the amount of gas demand measured by gas flow rate may increase, compared with the traditional natural gas systems. Nonetheless, the energy of the gas demands in the two cases should be the same. Thus, we have:

$$
\sum_{n \in \mathcal{N}} GCV_n q_{i,k,n}^d = GCV^{ng} q_{i,k}^{d,ng} \tag{5}
$$

$$
q_{i,k,n}^d / \sum_{n \in \mathcal{N}} q_{i,k,n}^d = \chi_{i,k,n} \tag{6}
$$

where GCV_n is the GCV of gas composition n; GCV^{ng} is the GCV of natural gas; $q_{i,k,n}^d$ is the gas demand of gas component n at bus i in dispatch interval k; $q_{i,k}^{d,ng}$ is the total gas demand at bus i in dispatch interval k if supplied with pure natural gas; $\chi_{i,k,n}$ is the molar fraction of gas component n at bus i in dispatch interval k.

The gases from gas sources are transported to gas demands by the pipeline network. The gas pressure drop and the gas flow can be described by the Weymouth equation (7). The gas flow is the sum of the gas flows of all components, as shown in (8). Due to the hydrogen blending, the gas constant $r_{ij,k}$ now varies with the dispatch interval k. Thus, in the Weymouth equation, the pressure square drop no longer has a linear relationship with the square of gas flow. The gas constant is associated with gas composition, as calculated by (9). Moreover, the gas composition of the gas mixture in the pipeline should inherit from the corresponding upper stream bus, as shown in (10). The gas flow and pressure should also be limited within the lower and upper bounds, as shown in (11) - (13).

$$
p_{i,k}^2 - p_{j,k}^2 = \gamma_{ij} \Theta_{ij}^2 r_{ij,k} q_{ij,k}^2 \tag{7}
$$

$$
\sum_{n \in \mathcal{N}} q_{ij,k,n} = q_{ij,k} \tag{8}
$$

$$
r_{ij,k} = \sum_{n \in \mathcal{N}} R_n \chi_{ij,k,n} \tag{9}
$$

$$
q_{ij,k,n} / q_{ij,k} = ((1 + \gamma_{ij}) \chi_{i,k,n} + (1 - \gamma_{ij}) \chi_{j,k,n}) / 2 \tag{10}
$$

$$
(\gamma_{ij} - 1) q_{ij}^{max} / 2 \le q_{ij,k} \le (\gamma_{ij} + 1) q_{ij}^{max} / 2 \tag{11}
$$

$$
(\gamma_{ij} - 1) q_{ij}^{max} / 2 \le q_{ij,k,n} \le (\gamma_{ij} + 1) q_{ij}^{max} / 2 \tag{12}
$$

$$
p_i^{min} \le p_{i,k} \le p_i^{max} \tag{13}
$$

where $p_{i,k}$ is the gas pressure at bus i in dispatch interval k,

respectively; γ_{ij} is the direction of gas flow, where $\gamma_{ij} = 1$ indicates that gas flows from bus i to j, and $\gamma_{ij} = -1$ indicates otherwise; $\Theta_{ij}^2 = \frac{16 f_{ij} (\rho^{ng,stp})^2 T^{ng} L_{ij} z^{ng}}{\pi D_{ij}^5}$ is the property coefficient of the Weymouth equation, where f_{ij}, L_{ij}, and D_{ij} are the friction factor, length, and diameter of pipeline ij, respectively; T^{ng} is the temperature of the gas, which is assumed to be constant in the system during the operation; ρ^{ng} is the gas density at the standard temperature and pressure conditions; z^{ng} is the compressibility factor, which almost does not change with gas composition; $q_{ij,k,n}$ is the gas flow rate of gas component n in pipeline ij at dispatch interval k; $q_{ij,k}$ is the gas flow for all gas components at dispatch interval k; R_n is the gas constant of gas component n; q_{ij}^{max} is the capacity of the pipeline ij; p_i^{min} and p_i^{max} are the lower and upper bounds of the gas pressure, respectively.

During transmission, different gas components may be mixed in a single bus and then transported to downstream locations. Then, the gas composition at the gas bus can be calculated by:

$$\chi_{i,k,n} = \left(\sum_{s \in \mathcal{S}_i} q_{i,s,k,n}^{gs} + \sum_{h \in \mathcal{H}_i} q_{i,h,k,n}^{ptg} + \sum_{j \in \mathcal{J}_i} \frac{1 - \gamma_{ij}}{2} q_{ij,k,n} \right)$$
$$/ \left(\sum_{s \in \mathcal{S}_i} q_{i,s,k}^{gs} + \sum_{h \in \mathcal{H}_i} q_{i,h,k}^{ptg} + \sum_{j \in \mathcal{J}_i} \frac{1 - \gamma_{ij}}{2} q_{ij,k} \right) \quad (14)$$

where $q_{i,h,k,n}^{ptg}$ is the production of gas component n of PTG h in bus i at dispatch interval k; It can represent either methane production $q_{i,h,k}^{me}$ when $n = 1$, or hydrogen production $q_{i,h,k}^{hy}$ when $n = 5$; $\mathcal{J}_i$ is the set of buses that are connected to bus i. The gas flow direction γ_{ij} is prespecified by solving the optimal energy flow problem with hydrogen injection replaced by natural gas, and thus the above equation only contains bilinear terms [39].

During the mixing process, the nodal gas balancing should be met (for $\forall n \in \mathcal{N}$):

$$\sum_{s \in \mathcal{S}_i} q_{i,s,k,n}^{gs} + \sum_{h \in \mathcal{H}_i} q_{i,h,k,n}^{ptg} + \sum_{j \in \mathcal{J}_i} \frac{1 - \gamma_{ij}}{2} q_{ij,k,n}$$
$$= \sum_{j \in \mathcal{J}_i} \frac{1 + \gamma_{ij}}{2} q_{ij,k,n} + \sum_{l \in \mathcal{L}_i^{gpp}} q_{i,l,k,n}^{gpp} + q_{i,k,n}^d : \lambda_{i,k,n}^g \quad (15)$$

where $\mathcal{L}_i^{gpp}$ is the set of gas-fired power plants at bus i; $q_{i,l,k,n}^{gpp}$ is the gas consumption of gas component n of gas-fired power plant l at bus i at dispatch interval k; $\lambda_{i,k,n}^g$ is the dual variable of constraints (15).

As the gas compositions fluctuate during the operation, they should be contained above a certain limit because excessive hydrogen injection may jeopardize the normal operation, and even the safety of H-IEGS. According to the recently amended Gas Safety (Management) Regulations [40], the Wobbe index (WI), flame speed factor (FS), relative density, and the molar fraction of hydrogen can serve as indices to regulate gas security. WI measures the heat energy output of gas appliances by consuming the same volume of the gas mixture at the same condition [41]. The operating conditions (such as rated gas flow rate) of gas appliances (such as gas water heaters) are usually tested under the same conditions. If the Wobbe index

is not consistent with hydrogen injection, then the gas water heater may not be able to reach the setting temperature at the rated gas flow rate. Therefore, limiting the value of WI is an important measure to ensure the normal functioning of gas systems under hydrogen injections. FS quantifies the speed at which a flame front travels through a fuel-air mixture. Therefore, the FS constraint is vital in ensuring stable combustion and avoiding flashbacks [42]. Therefore, we have (16)-(22):

$$RD_{i,k} = \sum_{n \in \mathcal{N}} \chi_{i,k,n} M_n / M^{air} \quad (16)$$

$$WI_{i,k} = \sum_{n \in \mathcal{N}} \chi_{i,k,n} GCV_n / \sqrt{RD_{i,k}} \quad (17)$$

$$FS_{i,k} = \frac{\sum_{n \in \mathcal{N}} \chi_{i,k,n} fs_n}{AF + 5\chi_{i,k}^{ni} - 18.8\chi_{i,k}^{ox} + 1} \quad (18)$$

$$0 \leq \chi_{i,k}^{hy} \leq \chi^{hy,max} \quad (19)$$

$$RD_{i,k} \leq RD^{max} \quad (20)$$

$$WI^{min} \leq WI_{i,k} \leq WI^{max} \quad (21)$$

$$FS^{min} \leq FS_{i,k} \leq FS^{max} \quad (22)$$

where $RD_{i,k}$, $WI_{i,k}$, and $FS_{i,k}$ are the relative density, WI, and FS of the gas mixture at bus i in dispatch interval k, respectively; M_n is the molecular weight of gas component n; M^{air} is the molecular weight of air; $\chi_{i,k}^{hy}$, $\chi_{i,k}^{ni}$, and $\chi_{i,k}^{ox}$ are the molar fractions of hydrogen, nitrogen, and oxygen in bus i at dispatch interval k, respectively; fs_n is the flame speed factor of gas component n; AF is the air-fuel ratio; $\chi^{hy,max}$ and RD^{max} are the upper bounds of hydrogen molar fraction and relative density, respectively; WI^{min}, WI^{max}, FS^{min} and FS^{max} are the lower and upper bounds of WI and FS, respectively.

Moreover, considering the hydrogen injection could significantly change the GCVs and gas flow pattern, to maintain the robustness of the H-IEGS, the linepack energy level should be maintained above a certain level, as in (26). The calculation method is shown below, where (23) is the gas state equation, (24) calculates the average gas density in the pipeline, and (25) calculates the linepack energy. The derivation process of the two equations can be found in [43].

$$\rho_{i,k} = p_{i,k} / r_{i,k} z^{ng} T^{ng} \quad (23)$$

$$\rho_{ij,k} = \frac{2}{3} \left(\rho_{i,k} + \rho_{i,k} - \frac{\rho_{i,k} \rho_{i,k}}{\rho_{i,k} + \rho_{i,k}} \right) \quad (24)$$

$$\psi_{ij,k} = V_{ij} \sum_{n \in \mathcal{N}} GCV_n \chi_{ij,k,n} \rho_{ij,k} \quad (25)$$

$$\psi_{ij,k} \geq (1 - \alpha_{ij}) \psi_{ij}^* \quad (26)$$

where $\rho_{i,k}$ and $\rho_{ij,k}$ are the gas densities at bus i and in pipeline ij at dispatch interval k, respectively; $\psi_{ij,k}$ is the linepack energy of pipeline ij at dispatch interval k; V_{ij} is the volume of pipeline ij; α_{ij} is the linepack threshold; ψ_{ij}^* is the reference value for linepack energy.

B. Electricity system constraints

The DC power flow model is usually adopted in the transmission-level nodal price calculation in electricity sys-

tems for robustness and computation speed [44]:

$$\sum_{l \in \mathcal{L}_i^{tpp} \cup \mathcal{L}_i^{gpp} \cup \mathcal{L}_i^{rng}} g_{i,l,k} - g_{i,k}^d - \sum_{h \in \mathcal{H}_i} g_{i,h,k}^{ptg}$$

$$- \sum_{j \in \mathcal{J}_i} g_{ij,k} = 0 : \lambda_{i,k}^e \qquad (27)$$

$$g_{i,l,k}^{min} \le g_{i,l,k} \le g_{i,l,k}^{max}, l \in \mathcal{L}_i^{tpp} \cup \mathcal{L}_i^{rng} \qquad (28)$$

$$\theta_{i,k} - \theta_{j,k} = X_{ij} g_{ij,k} \qquad (29)$$

$$-g_{ij}^{max} \le g_{ij,k} \le g_{ij}^{max} \qquad (30)$$

where $\mathcal{L}_i^{rng}$ is the set of renewable generators in bus i; $g_{i,l,k}^{min}$ and $g_{i,l,k}^{max}$ are the minimum and maximum electricity generation of generator l in bus i, respectively (the renewable generation capacity is related to k); $g_{i,h,k}^{ptg,e}$ is the electricity consumption of PTG h at bus i at dispatch interval k; $g_{i,k}^d$ is the electricity demand in bus i at dispatch interval k; $g_{ij,k}$ is the electricity power flow in electric branch ij; $\lambda_{i,k}^e$ is the dual variable of constraint (27); $\theta_{i,k}$ is the voltage phase angle; X_{ij} is the reactance of electric branch ij; g_{ij}^{max} is the capacity of the branch.

C. Coupling constraints

Gas-fired power plant consumes gas from the gas system to generate electricity. Its energy conversion relationship can be represented by (31). The gas composition of the consumed gas should equal the gas composition at the corresponding bus as in (32). We assume the efficiency of the gas-fired power plant is constant. Then, its generating capacity depends on the maximum inlet flow rate and the GCV of gas mixtures. Therefore, the generating capacity of gas-fired power plants may change during the operation, as shown in (33).

$$g_{i,l,k}^{gpp} = \eta_{i,l}^{gpp} \sum_{n \in \mathcal{N}} GCV_n q_{i,l,k,n}^{gpp} \qquad (31)$$

$$q_{i,l,k,n}^{gpp} / \sum_{n \in \mathcal{N}} q_{i,l,k,n}^{gpp} = \chi_{i,k.n} \qquad (32)$$

$$g_{i,l}^{gpp,min} \le \eta_{i,l}^{gpp} GCV^{ng} \sum_{n \in \mathcal{N}} q_{i,l,k,n}^{gpp} \le g_{i,l}^{gpp,max} \qquad (33)$$

where $\eta_{i,l}^{gpp}$ is the energy conversion efficiency of gas-fired power plant l in bus i; $g_{i,l}^{gpp,min}$ and $g_{i,l}^{gpp,max}$ are the minimum and maximum electricity generation of gas-fired power plant l at bus i with original natural gas (without blending hydrogen).

PTG consumes electricity to produce synthetic gas. The energy conversion relationship and capacity can be calculated by:

$$q_{i,h,k}^{hy} GCV^{hy} + q_{i,h,k}^{me} GCV^{me} / \eta_{i,h}^{me} = g_{i,h,k}^{ptg} \eta_{i,h}^{el} \qquad (34)$$

$$g_{i,h,k}^{ptg} \le q_{i,h}^{hy,max} GCV^{hy} / \eta_{i,h}^{el} \qquad (35)$$

$$q_{i,h,k}^{me}, q_{i,h,k}^{hy} \ge 0 \qquad (36)$$

where $q_{i,h,k}^{hy}$ is the hydrogen production of PTG h in bus i at dispatch interval k, respectively; $\eta_{i,h}^{me}$ and $\eta_{i,h}^{el}$ are the energy conversion efficiencies in the methanation and electrolysis processes, respectively; GCV^{me} and GCV^{hy} are the GCVs of methane and hydrogen, respectively. Similarly, the carbon

capture factor $\beta_{i,h}$ equals M^{cd}, where M^{cd} is the molecular weight of carbon dioxide.

IV. SOLUTION METHOD

A. Solution method for nodal energy price

During the solution of the market clearing problem formulated in the last section, the dual variables can be calculated as the nodal energy prices. However, the above optimization problem is highly nonlinear and nonconvex. The nonlinearity is mainly caused by: i) The nonlinear terms in the calculation of linepack energy in (23) - (26); ii) the product of multiple decision variables in the Weymouth equation (7) with varying gas constants; iii) the bilinear terms in the gas mixing regarding the gas compositions (6), (10), (14), and (32); iv) the square of root term in Wobbe index in (17).

First, we linearize the Wobbe index constraint and the linepack energy constraints by first-order Taylor approximation as follows:

$$WI^{min} \le \frac{2GCV_{i,k}}{\left(\sqrt{RD^{ng}} + \frac{RD_{i,k}}{\sqrt{RD^{ng}}}\right)} \le WI^{max} \qquad (37)$$

$$V_{ij} \sum_{n \in \mathcal{N}} GCV_n(\chi_n^{ng}\rho^{ng} + (\chi_{ij,k,n} - \chi_n^{ng})\rho^{ng}$$

$$+\chi_n^{ng}(\rho_{ij,k} - \rho^{ng})) \ge (1 - \alpha_{ij})\psi_{ij}^* z^{ng} r_{ij} T^{ng}\rho^{ng} \qquad (38)$$

$$\rho_{ij,k} = \rho^{ng} + \frac{\partial \rho_{ij,k}}{\partial \rho_{i,k}}(\rho_{i,k} - \rho^{ng}) + \frac{\partial \rho_{ij,k}}{\partial \rho_{j,k}}(\rho_{j,k} - \rho^{ng}) \qquad (39)$$

where RD^{ng}, ρ^{ng}, and χ_n^{ng} are the relative density, gas density, and gas composition of natural gas, respectively.

Then, the market clearing problem can be preliminarily simplified into a quadratic programming problem with quadratic equality constraints (the gas constant in (7) is tentatively regarded as a constant here). It can be written in the following compact form:

$$\min_{\boldsymbol{u}} \boldsymbol{u}^T \boldsymbol{Q} \boldsymbol{u} + \boldsymbol{c}^T \boldsymbol{u} \qquad (40)$$

subject to:

$$\boldsymbol{u}^T \boldsymbol{P} \boldsymbol{u} + \boldsymbol{A} \boldsymbol{u} + \boldsymbol{b} = 0 \qquad (41)$$

$$\boldsymbol{C} \boldsymbol{p}^2 + \boldsymbol{\gamma} \boldsymbol{D} \boldsymbol{q}^2 = 0 \qquad (42)$$

$$\boldsymbol{E} \boldsymbol{u} + \boldsymbol{f} \le 0 \qquad (43)$$

where (41), (42), and (43) represent the bilinear constraints, Weymouth equation constraints, and linear constraints in the market clearing problem, respectively; (41) corresponds to (6), (14), (23)-(26), and (32); (42) corresponds to (7); (43) is corresponding to the rest of the constraints, i.e., (2)-(5), (8)-(13), (15), (16), (18)-(22), (27)-(31), (33)-(36); $\boldsymbol{u}$ is the set of decision variables; $\boldsymbol{p}$ and $\boldsymbol{q}$ represent the sets of pressures and gas flows, respectively; $\boldsymbol{P}$, $\boldsymbol{Q}$, $\boldsymbol{c}$, $\boldsymbol{A}$, $\boldsymbol{b}$, $\boldsymbol{C}$, $\boldsymbol{D}$, $\boldsymbol{E}$ and $\boldsymbol{f}$ are the coefficient matrices.

Due to the quadratic equality constraints, the optimization problem still can not be tractable solved. However, we note that the epigraph of constraints (41) and (42) on their domains are convex. Then, we can solve it by using successive second-

order cone programming (SSOCP). For example, (41) can be linearized as:

$$\hat{\boldsymbol{u}}^T \boldsymbol{P} \hat{\boldsymbol{u}} + \nabla(\boldsymbol{u}^T \boldsymbol{P} \boldsymbol{u})(\boldsymbol{u} - \hat{\boldsymbol{u}}) + \boldsymbol{A}\boldsymbol{u} + \boldsymbol{b} + \boldsymbol{\delta}^{mx} = 0 \quad (44)$$

where $\hat{\boldsymbol{u}}$ is the set of reference points; $\boldsymbol{\delta}^{mx}$ is the set of Taylor series remainders for this constraint.

For the reformulated Weymouth equation, we can approximate it by a convex-concave procedure:

$$\boldsymbol{C}\boldsymbol{p}^2 + \boldsymbol{D}\boldsymbol{q}^2 \leq 0 \quad (45)$$

$$\boldsymbol{C}\hat{\boldsymbol{p}}(\boldsymbol{p}-\hat{\boldsymbol{p}}) + \boldsymbol{D}\hat{\boldsymbol{q}}(\boldsymbol{q}-\hat{\boldsymbol{q}}) + \boldsymbol{\delta}^{wm} \geq 0 \quad (46)$$

where $\hat{\boldsymbol{p}}$ and $\hat{\boldsymbol{q}}$ are the reference points of gas pressure and gas flow, respectively; $\boldsymbol{\delta}^{wm}$ is the set of Taylor series remainders.

Adding the slack variable to the objective function, we obtain the new optimization problem in a second-order cone form:

$$\min_{\boldsymbol{u},\boldsymbol{\delta}} \boldsymbol{u}^T \boldsymbol{Q} \boldsymbol{u} + \boldsymbol{c}^T \boldsymbol{u} + \boldsymbol{\varphi}(\boldsymbol{1}^T \boldsymbol{\delta}) \quad (47)$$

subject to:

$$\boldsymbol{A}'\boldsymbol{u} + \boldsymbol{b}' \geq \boldsymbol{0} : \boldsymbol{\lambda} \quad (48)$$

$$||\boldsymbol{c}'_m \boldsymbol{u}_m + \boldsymbol{d}'_m||_2 \leq \boldsymbol{e}'_m \boldsymbol{u}_m + \boldsymbol{f}'_m : \boldsymbol{\nu}, \boldsymbol{\omega}, \forall m \in \mathcal{M}_{SOC} \quad (49)$$

where $\boldsymbol{A}'$, $\boldsymbol{b}'$, $\boldsymbol{c}'_m$, $\boldsymbol{d}'_m$, $\boldsymbol{e}'_m$, and $\boldsymbol{f}'_m$ are the updated coefficient matrices in m_{th} second-order cone constraint; $\boldsymbol{\varphi}$ is the set of penalty coefficients; $\boldsymbol{\delta} = \{\boldsymbol{\delta}^{mx}, \boldsymbol{\delta}^{wm}\}$ is the set of slack variables; $\mathcal{M}_{SOC}$ is the set of second-order cone constraints; $\boldsymbol{\lambda}$ is the set of dual variables for linear constraints; $\boldsymbol{\nu}$ and $\boldsymbol{\omega}$ are the sets of dual variables for second-order cone constraints.

Accordingly, the dual problem can be obtained as:

$$\min \frac{1}{4}\boldsymbol{\lambda}^T \boldsymbol{A}' \boldsymbol{Q}^{-1} \boldsymbol{A}'^T \boldsymbol{\lambda} + (\boldsymbol{c}^T \boldsymbol{Q}^{-1} \boldsymbol{A}'^T + \boldsymbol{b}'^T)\boldsymbol{\lambda} +$$
$$\sum_{m \in \mathcal{M}_{SOC}} (\boldsymbol{\mu}_m \boldsymbol{d}'_m + \boldsymbol{\omega} \boldsymbol{f}'_m) \quad (50)$$

subject to:

$$\boldsymbol{c}' = \boldsymbol{A}'^T \boldsymbol{\lambda} + \sum_{m \in \mathcal{M}_{SOC}} (\boldsymbol{c}'_m \boldsymbol{\nu} + \boldsymbol{e}'_m \boldsymbol{\omega}) \quad (51)$$

$$\boldsymbol{\lambda} \geq \boldsymbol{0}, \; ||\boldsymbol{\nu}_m||_2 \leq \boldsymbol{\omega}_m \quad (52)$$

The nodal energy price can be obtained by solving the above dual problem. The detailed procedures are illustrated in the next subsection.

B. Warm-start for continuous market clearing

The convergence efficiency of SSOCP in the last subsection depends on the initial reference points of the decision variables (e.g., $\hat{\boldsymbol{u}}$). Besides adding penalty factors in the objective functions (e.g., $\boldsymbol{p}^2$ or $\boldsymbol{q}^2$) as previous research does, we propose a warm-start method to facilitate convergence during continuous market clearing. The basic idea of this method is to use the information in former operation periods to select initial values closer to optimal points. By this means, the computation efficiency can be improved without sacrificing accuracy.

For the market clearing problem at each dispatch interval k, we look for similar renewable generation and load patterns that have appeared in the previous dispatch interval κ. Initially,

---

Algorithm 1 SSOCP for market clearing in H-IEGS

Initialize the iteration indicator $\iota = 0$; Initialize the penalty factor φ^ι. Set the maximum penalty factor as φ^{max}. Set the multiplier for the penalty factor in each iteration as ϑ; Set the convergence criterion as ϵ; Initialize the value of gap, $gap > \epsilon$.

Solve optimization problem (47)-(49) at the base scenario, and obtain the system state as $\boldsymbol{x}_0$.

for $k \in \mathcal{K}$ **do**
    if $k = 1$ **then**
        Set initial reference points according to $\boldsymbol{x}_0$
    else
        Set initial reference points according to (56) and (57).
    end if
    while $gap > \epsilon$ **do**
        Solve the optimal energy flow problem by assuming the homogeneous gas composition to obtain the gas flow direction γ_{ij} [45].
        Solve optimization problem (47)-(49) to obtain the state of the H-IEGS, denoted as $\boldsymbol{x}^\iota$.
        Calculate the gap as:

$$gap = \frac{2|\boldsymbol{x}^\iota - \boldsymbol{x}^{\iota-1}|}{\boldsymbol{x}^\iota + \boldsymbol{x}^{\iota-1}} \quad (53)$$

        if $gap < \epsilon$ **then**
            Solve the dual problem (50)-(52). Obtain the dual variables λ_i^e and $\lambda_{i,k,n}^g$. The nodal electricity price is $\lambda_{i,k}^e$; the nodal gas price is calculated by:

$$\lambda_{i,k}^g = \sum_{n \in \mathcal{N}} \chi_{i,k,n} \lambda_{i,k,n}^g \quad (54)$$

        else
            Update the penalty factor as:

$$\varphi^{\iota+1} = \min\{\vartheta\varphi^\iota, \varphi^{max}\} \quad (55)$$

            Update the reference point $\hat{\boldsymbol{u}}^\iota$ as $\hat{\boldsymbol{u}}$; update gas constant $\boldsymbol{r}^\iota$ as the reference point $\hat{\boldsymbol{r}}$ in the Weymouth equation (7).
        end if
    end while
end for

---

we have a base scenario where the wind generation and energy loads are at their rated values, and the operating state of the H-IEGS is denoted as $\boldsymbol{x}_0$. Take wind generation as an example. In the market clearing problem in dispatch interval k, we have a set of renewable generating capacities $\boldsymbol{g}_k^{rng}$ = $\left\{g_{i,l,k}^{rng,max}, i \in \mathcal{I}, l \in \mathcal{L}_i^{rng}\right\}$. For each dispatch interval k, we calculate the distance between the wind generation at the current dispatch interval k and previous dispatch interval κ (if $k = 1$, we calculate the weighted distance between k and the base scenario):

$$d_{k,\kappa}^{rng} = ||\boldsymbol{g}_k^{rng} - \boldsymbol{g}_\kappa^{rng}||/||\boldsymbol{g}^{rt}|| \quad (56)$$

where $d_{k,\kappa}^{rng}$ is the distance between the wind generation of

Fig. 4. H-IEGS test system.

Fig. 5. Convergence of SSOCP.

Fig. 6. Computation errors with respect to different gas components.
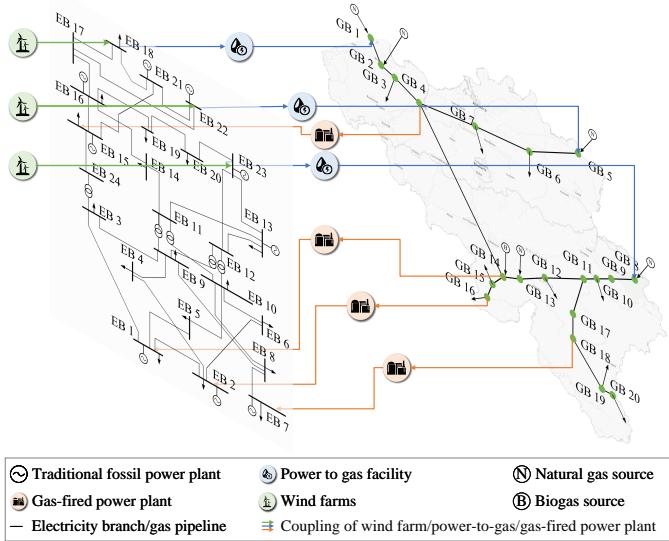
k and κ; g^{rt} is the rated power of renewable generation. The weighted distance of energy demands can be calculated similarly.

The energy demands mainly influence the gas pressure and gas flow, while wind generation usually influences the gas composition. Taking the initial reference point of gas composition as an example, we can calculate it by:

$$\hat{\chi}_k = \sum_{\kappa=1}^{k} \frac{e^{-d_\kappa^{rng}}}{\sum_{\kappa=1}^{k} e^{-d_\kappa^{rng}}} \chi_\kappa \tag{57}$$

where χ_κ is the solution of χ at dispatch interval κ.

The specific SSOCP procedures for the market clearing problem with the proposed warm-start method are illustrated in Algorithm 1.

V. CASE STUDIES

An H-IEGS test case, consisting of IEEE 24 RTS and Belgium natural gas transmission system is used to validate the proposed method [46], [47]. The topological structure of the test system is shown in Fig. 4. The two energy systems are tightly coupled by PTGs and gas-fired power plants. Three wind farms are located at electricity bus #18, #22, and #23, respectively. Three PTGs connect electricity bus #18 and gas bus #1, electricity bus #22 and gas bus #5, and electricity bus #23 and gas bus #8, respectively. The gas compositions of gas sources are set according to [48].

A. Validation of proposed methods

In this subsection, the proposed SSOCP method is validated. We assume all the wind farms operate at their rated power.

The convergence curve is shown in Fig. 5. As we can see, the algorithm converges after five iterations (the convergence criterion is set to 10^{-3}). The computation time is 0.47s, which is 96.90% higher than the traditional nonlinear solver (the computation time of the IPOPT solver is 15.16s). The computation accuracy is also compared in Fig. 6. The relative
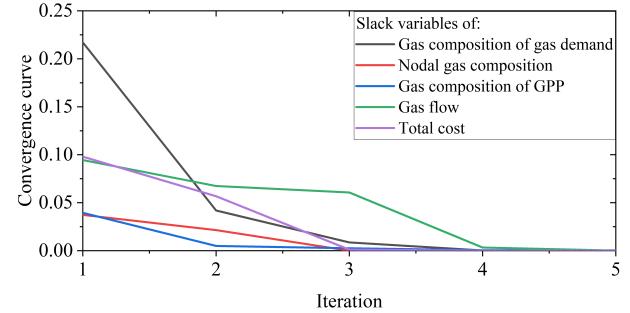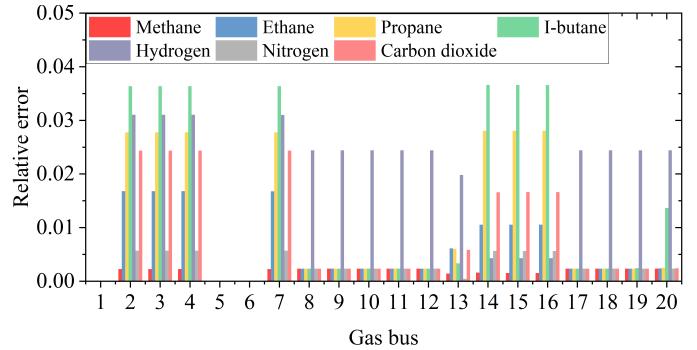
errors at all buses can be controlled within 4% compared with the results of the nonlinear solver, demonstrating a very satisfying accuracy.

Then, the effectiveness of the proposed nodal energy price scheme is also validated, as shown in Fig. 7. Two scenarios are set. In S1, the blending of hydrogen is considered. In S2, the hydrogen is not blended with the gas system, which means the gas compositions are homogeneous across the gas network.

Fig. 7 (a) shows the nodal electricity prices. Firstly, we can find the spatial difference in electricity prices. Some electricity buses (e.g., #17, #18, #21, #22, etc.) have significantly lower electricity prices than other buses. This is because these buses are near wind farms with lower generation costs. Thus, their marginal generators have lower generating costs. For example, the marginal unit of electricity bus #17 is the generator #23 at electricity bus #18, the marginal cost of which is around 2 $/MW, as shown in Fig. 7 (b). Comparing S1 and S2, we can find that the nodal electricity prices with hydrogen blending are slightly higher than those without hydrogen blending. For example, the average system electricity price in S1 is 3.35% higher than in S2, and the nodal electricity price at #19 in S1 is 9.72% higher than in S2. This is because when PTGs are used to produce hydrogen, the system electricity load will increase slightly, thus increasing the marginal cost. Particularly, in the electricity buses near PTG locations and without direct connection with wind farms (such as electricity bus #19), this impact will be more significant.

The nodal gas price scheme is more complicated than the electricity price due to the variation in the physical properties of the gas. To derive the nodal gas price, we first calculate the nodal gas composition distributions across the gas network. The gas productions of different gas sources and PTGs with

(a)

(b)

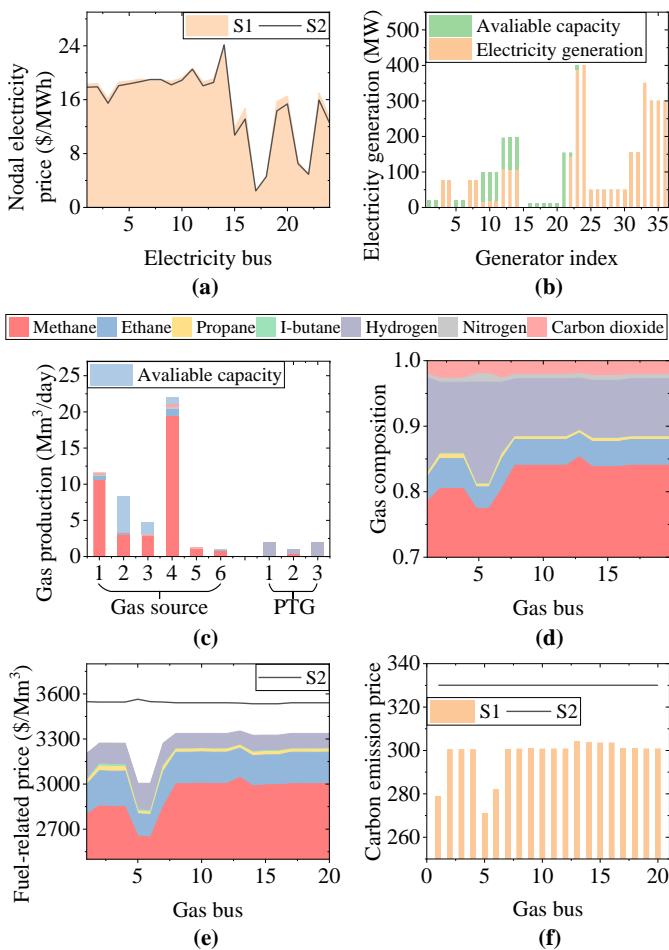**(c)**

(d)

(e)

(f)

Fig. 7. Nodal energy prices: (a) nodal electricity price; (b) operating states of generators; (c) fuel-related price in the nodal gas price; (d) operating state of gas sources and PTGs; (e) nodal gas composition; (f) carbon emission price in the nodal gas price.

various gas compositions lead to different nodal gas compositions, as shown in Fig. 7 (c). As we can see, the gas sources mainly comprise methane, while the PTG production mainly comprises hydrogen. Three PTGs all operate at their maximum capacity. PTGs #1 and #3 produce hydrogen, and PTG #2 further converts the hydrogen into methane due to the gas security limits. Due to the hydrogen injections by PTGs, the hydrogen fraction in the gas system is around 8.8%, while at some gas buses, such as #5 and #6, the hydrogen fractions can reach 15.49%, as shown in Fig. 7 (d).

The nodal gas price can be decomposed into two parts, fuel-related price (the part of the nodal gas price that is driven by the gas production cost of gas sources), and carbon emission price (the part of the nodal gas price that is driven by the carbon emission cost). Fig. 7 (e) shows the fuel-related price. Generally, the nodal fuel-related price aligns with the nodal hydrogen proportion. For example, at gas buses #5 and #6 where the hydrogen proportion is high, the nodal gas prices are lower (8.48% lower than the system average price). By further decomposing the cost based on different gas components, we can see that methane is the main driving factor for gas prices, which takes 89.17% of gas prices. Then, there are ethane, hydrogen, propane, and I-butane, respectively. Because
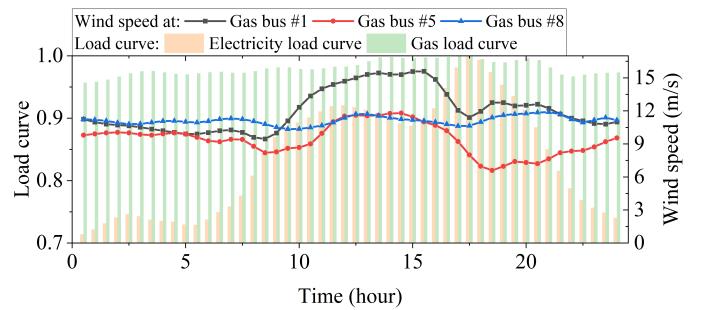

Fig. 8. Electricity and gas load curves and wind speeds.

nitrogen and carbon dioxide do not provide heat energy, their contributions to the nodal gas price are near zero. Compared with S2, the nodal fuel-related price in S1 is significantly lower by 7.34%. This is because most hydrogen in S1 is produced by consuming surplus renewable energy with nearly zero marginal cost.

Fig. 7 (f) shows the carbon emission price (the total nodal gas price can be obtained by adding the fuel-related price and carbon emission price in Fig. 7 (e) and Fig. 7 (f), respectively). We find that the carbon emission price also aligns well with the molar fraction of hydrogen. For example, the carbon emission price of gas bus #5 is the lowest among all buses. This is because hydrogen contributes more to the gas demand at gas bus #5. With less carbon content, gas bus #5 will produce less carbon dioxide by consuming the same volume of gas. Compared to the pure gas system, the carbon emission price in H-IEGS can be reduced by 9.75%. This validates the effectiveness of hydrogen blending in saving both the operation cost and carbon emission.

B. Continuous operation and impact factor analysis of nodal energy price

In this subsection, we first demonstrate the performance of nodal energy prices in the practical daily continuous operation. The energy load profiles are obtained from Australian Energy Market Operator [49], as shown in Fig. 8. The wind speed data are obtained from the National Oceanic and Atmospheric Administration [50], where the weather stations share similar geographical locations as in the Belgium gas transmission system.

Fig. 9 (a) shows the nodal electricity prices during the daily operation. We find that the nodal electricity price varies both spatially and temporally. The highest electricity price is 27.45 $/MWh, appearing at electricity bus #14 at 17:30. This is because electricity bus #14 is congested with a high-cost generating unit, and the electricity load at that time is high. Similarly, the lowest electricity price is 2.06 $/MWh, appearing at electricity bus #17 at 16:30. Thus, in the time dimension, we can assert that the electricity price varies with the changes in load patterns and wind speed. However, the temporal patterns at different buses are different. Here we take electricity buses #14, #16, and #17 as examples, as shown in Fig. 9 (b). The electricity price of electricity bus #14 mainly follows the load curve, e.g., the price peak appears at 17:30. In contrast, the electricity price of electricity bus #17 follows the wind speed curve, e.g., the price valley appears at 11:00-16:30.

This article has been accepted for publication in IEEE Transactions on Sustainable Energy. This is the author's version which has not been fully edited and content may change prior to final publication. Citation information: DOI 10.1109/TSTE.2024.3372628
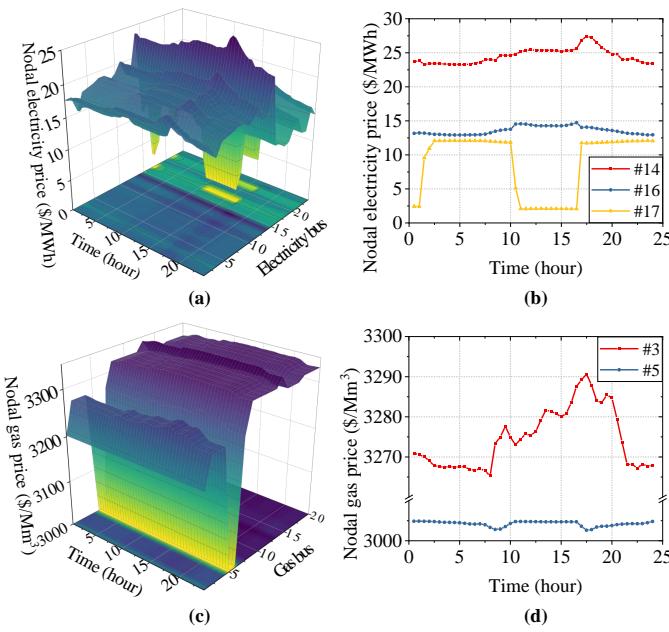
11

Fig. 9. Nodal energy prices during continuous operation: (a) Nodal electricity price; (b) electricity prices at electricity bus #14, #16, and #17; (c) nodal gas price; (d) gas prices at gas bus #3 and #5.

TABLE II
SCENARIO SETTINGS FOR SENSITIVITY ANALYSIS

	Tight	Medium	Relaxed
FS	$[0.9FS^{ng}, 1.1FS^{ng}]$	$[0.8FS^{ng}, 1.2FS^{ng}]$	$[0.7FS^{ng}, 1.3FS^{ng}]$
WI	[47.2,51.41] MJ/m^3	[46.5,52.85] MJ/m^3	[45.8,54.29] MJ/m^3

FS^{ng} is the flame speed factor of the original natural gas.

Fig. 9(c) shows the nodal gas price during the daily operation. The highest nodal gas price is 3355 \$/Mm^3, appearing at gas bus #13 at 13:30, while the lowest nodal gas price is 3003 \$/Mm^3, appearing at gas bus #6 at 17:30. We can find that the gas price pattern is significantly different from the electricity price. The temporal differences in gas prices are almost negligible compared with the spatial differences. This is because the gas flow pattern is relatively more stationary than the electricity flow. Thus, the changes in wind generation and energy demand merely affect the gas flow pattern and marginal cost. However, there still exist different temporal patterns of gas prices at different gas buses, as shown in Fig. 9 (d). The gas price at gas bus #3 fluctuates more intensively over time compared with gas bus #5. This is because a PTG is located at gas bus #5. No matter how the gas demand fluctuates, the hydrogen production capacity of the PTG can basically cover this fluctuation and guarantee a relatively steady hydrogen proportion. Thus, the gas price at gas bus #5 is stationary. In contrast, the gas demand at gas bus #3 is mainly supplied by different gas sources. Their outputs vary with the gas load level. Thus, the nodal gas price at gas bus #3 is more fluctuated.

Through the case above, we know the impacts of wind levels and load levels on the nodal energy prices during continuous operation. Considering the policy regulations on the gas properties in the H-IEGS have not been finalized yet, here we further conduct sensitivity analysis towards the
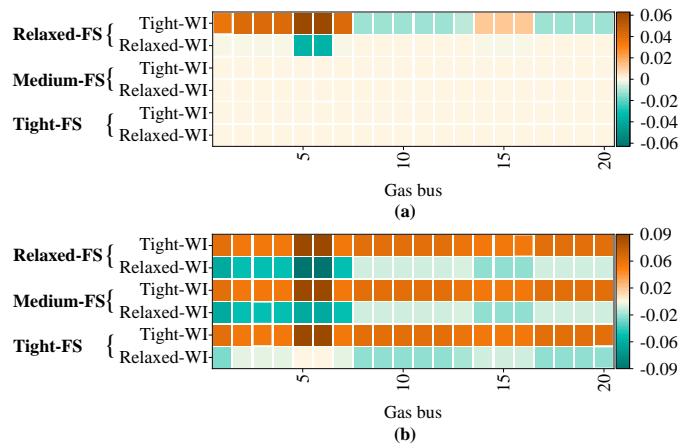

Fig. 10. Sensitivity analysis of nodal gas price: (a) impact of WI; (b) impact of FS.

security constraints of gas composition. Different upper and lower limits of the Wobbe index and flame speed factor are set according to practical gas safety regulations [51], namely, tight, medium, and relaxed, as presented in Table. II. For example, the scenario with tight FS and relaxed WI constraints are denoted as "tight-FS" and "relaxed-WI", respectively. Since the gas constraints mainly affect nodal gas prices other than electricity prices, we mainly focus on the sensitivities of nodal gas prices.

Fig. 10. (a) shows the impact of WI (including the tightening of WI constraints and the relaxation of WI constraints) in different scenarios (including tight FS constraint scenario, middle FS constraint scenario, and relaxed FS constraint scenario). We can find that when FS constraints are set to ±10% and ±20%, the WI limits merely affect the nodal gas price. This is because, in these scenarios, the hydrogen compositions are mainly restrained by the FS limit. When the FS limit further increases to ±30%, WI begins to show impacts on the nodal gas price, especially on gas bus #5 and #6. It may cause the gas price to increase by up to 6%. This is because the gas source at gas bus #5 is relatively small, and thus the gas bus #5 and #6 are easier to violate the WI constraints with the hydrogen injection by PTG. The downstream gas buses, such as #8-#13, on the other hand, are less affected.

Fig. 10. (b) shows the impacts of FS constraints with different WI limits. We can observe a clear pattern that the tightening of FS will increase the nodal gas price, while the relaxation of FS will decrease the nodal gas price in all scenarios. This is because the relaxation of FS limits will allow more injections of green hydrogens from low-cost renewable generations. Moreover, the impacts of FS on the nodal gas price can reach 9%, which is more significant than those of WI.

C. Validation using a large case

In this case, we further validate the scalability of our proposed method using a large case. They are real electricity and gas systems from northwest China, consisting of 165 electricity buses and 171 gas buses [52]. The total computation time is 138.96s.
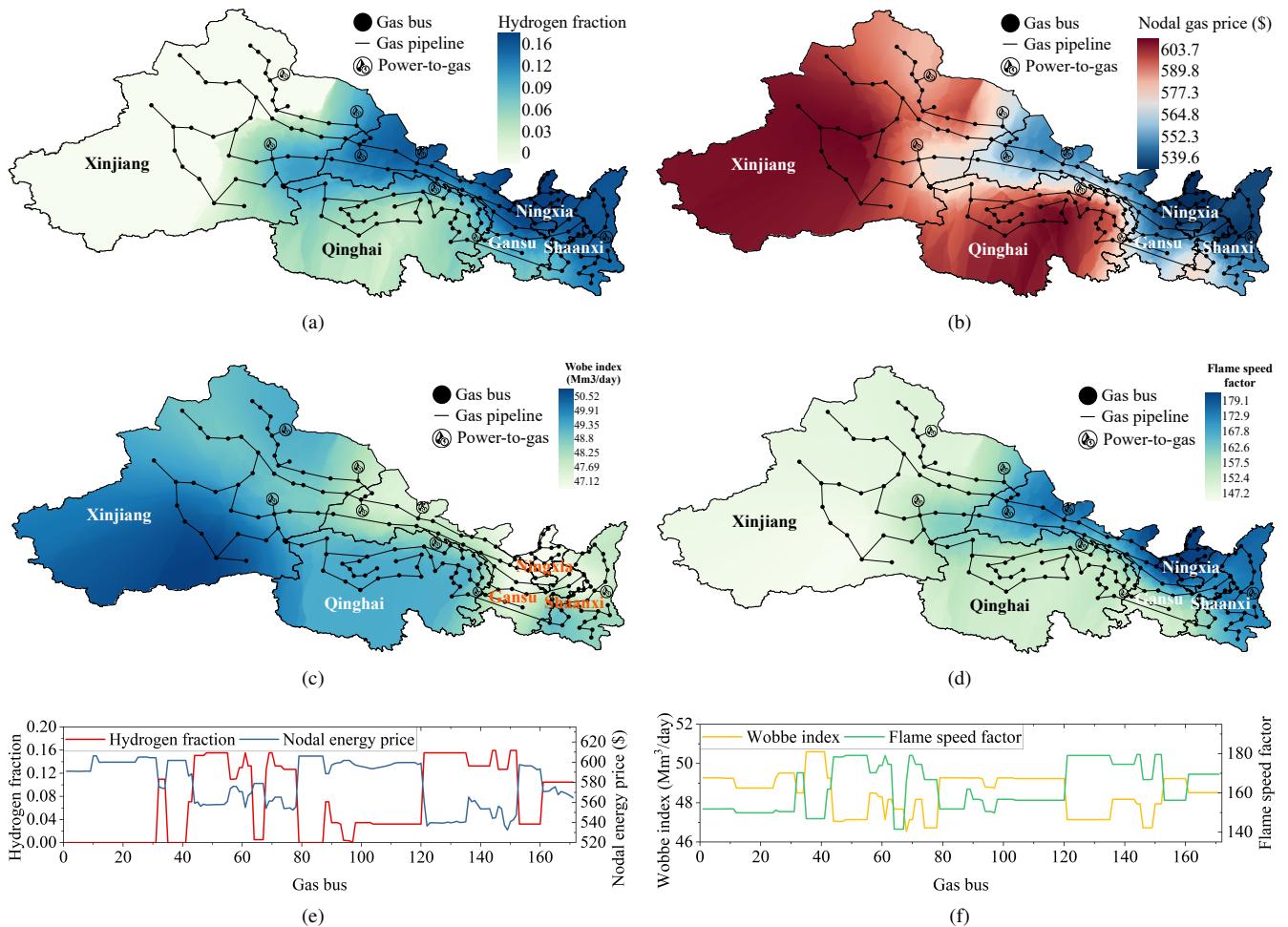
Fig. 11. China's Northwest H-IEGS: (a) hydrogen fraction; (b) nodal gas price; (c) Wobbe index; (d) flame speed factor; (e) hydrogen fraction and nodal gas price; (f) Wobbe index and flame speed factor.

The nodal hydrogen compositions, nodal gas prices, and gas security indices are presented in Fig. 11. We can find that the hydrogen fractions generally increase from west to east. Their values are higher in Northern Gansu, Ningxia, and Northern Shanxi provinces than in other locations. This is because the gas flows basically from west to east, and the wind farms are mainly located in the middle Ningxia, North Shanxi, and Gansu areas. Thus, the PTGs at these locations that are closer to the renewable generations tend to produce hydrogen. We can also observe that the nodal gas price distribution presents a very similar pattern to the hydrogen fraction. This also owes to the lower marginal cost of hydrogen. As a result, the nodal gas prices in Gansu, Ningxia, and Shanxi provinces are lower than in other locations.

The WI generally presents the opposite pattern to the hydrogen fraction. In Xinjiang and Qinghai these provinces where hydrogen fraction is lower, the WI is higher. The flame speed factor, on the contrary, generally grows with the increase in hydrogen fraction. We can observe from Fig. 11. (f) that some places, such as gas buses #146-148 in Ningxia provinces, have the lowest WI, which means we should pay attention to the gas qualities. However, as also shown in Fig. 11. (e), these areas do not necessarily have the highest hydrogen fractions

flame speed factors, or lowest gas prices. This means the gas quality and nodal gas price of the gas mixtures are not monotonically determined by hydrogen fraction, but are jointly determined by hydrogen and the quality of natural gas sources. This further demonstrates the complexity of this problem and the necessity of the qualitative method in this paper.

VI. CONCLUSIONS

This paper proposes a novel nodal energy price scheme for hydrogen-blended integrated electricity and gas systems considering the heterogeneous gas compositions. By numerical studies, we validated that compared with the traditional nodal energy price scheme, the proposed one can reflect the impacts of hydrogen blending (e.g., lower GCV, cost, carbon emission, etc.) in the nodal energy price. By blending the hydrogen, the system's gas price and carbon emission price can be reduced by 8.48% and 9.75%, respectively. It validates that our scheme can both reflect the impacts of the inconsistent GCV and values of decarbonization by the hydrogen injection, which could provide more incentives in future market operations. Moreover, we identified the major constraints on the gas quality (such as the Wobbe index, flame speed factor, etc.) which significantly influence the temporal and spatial patterns

of nodal energy prices. If the gas security constraints are further relaxed due to technical advancement, the nodal energy price can decrease by 9%, which further reveals the value of hydrogen blending in the energy system decarbonization. We further validate the scalability of the proposed method using a practical large-scale H-IEGS. The proposed method can help the system operator evaluate the probable energy price distributions in the future energy system if green hydrogen is widely blended and causes heterogeneous gas compositions.

REFERENCES

[1] Hydrogen blending into gb gas distribution networks. [Online]. Available: https://assets.publishing. service.gov.uk/media/657a0a82254aaa0010050cde/ hydrogen-blending-strategic-policy-decision.pdf.

[2] Hyblend: Opportunities for hydrogen blending in natural gas pipelines. [Online]. Available: https://www.energy.gov/eere/fuelcells/ hyblend-opportunities-hydrogen-blending-natural-gas-pipelines.

[3] EU hydrogen policy. [Online]. Available: https://www.europarl.europa. eu/RegData/etudes/BRIE/2021/689332/EPRS_BRI(2021)689332_EN. pdf.

[4] UK hydrogen strategy. [Online]. Available: https://www.gov.uk/ government/publications/uk-hydrogen-strategy.

[5] The National Hydrogen Strategy. [Online]. Available: https://www.bmbf.de/bmbf/shareddocs/downloads/files/bmwi_ nationale-wasserstoffstrategie_eng_s01.pdf?__blob=publicationFile&v= 1.

[6] Naturalhy. [Online]. Available: https://www.gerg.eu/projects/hydrogen/ naturalhy/.

[7] The grhyd demonstration project. [Online]. Available: https://www.engie.com/en/businesses/gas/hydrogen/power-to-gas/ the-grhyd-demonstration-project.

[8] Italy's snam in world first with test of 30

[9] Hydeploy. [Online]. Available: https://hydeploy.co.uk/.

[10] Hynet. [Online]. Available: https://hynet.co.uk/.

[11] Futuregrid. [Online]. Available: https://www.nationalgas.com/ insight-and-innovation/transmission-innovation/futuregrid.

[12] U.S. National Clean Hydrogen Strategy and Roadmap. [Online]. Available: https://www.hydrogen.energy.gov/library/roadmaps-vision/ clean-hydrogen-strategy-roadmap.

[13] Safe operation for one year with 10

[14] Launch of hebei's first demonstration project on natural gas with hydrogen blending (in chinese). [Online]. Available: https://news.bjx. com.cn/html/20200917/1105156.shtml.

[15] Technical status and prospects of hydrogen pipeline (in chinese). [Online]. Available: http://www.chinaden.cn/news_nr.asp?id=31208& Small_Class=3.

[16] Australia's national hydrogen strategy. [Online]. Available: https://www.dcceew.gov.au/energy/publications/ australias-national-hydrogen-strategy.

[17] Hydrogen park south australia. [Online]. Available: https://www.agig. com.au/hydrogen-park-south-australia.

[18] Britain's hydrogen blending delivery plan. [Online]. Available: https: //hydeploy.co.uk/app/uploads/2022/06/HyDeploy-Close-Down-Report_ Final.pdf.

[19] P. Wang, Y. Xiao, and Y. Ding, "Nodal market power assessment in electricity markets," *IEEE Transactions on Power Systems*, vol. 19, no. 3, pp. 1373–1379, Aug. 2004.

[20] P. M. Sotkiewicz and J. M. Vignolo, "Nodal pricing for distribution networks: efficient pricing for efficiency enhancing dg," *IEEE transactions on power systems*, vol. 21, no. 2, pp. 1013–1014, May. 2006.

[21] S. Yang, K.-W. Lao, Y. Chen, and H. Hui, "Resilient distributed control against false data injection attacks for demand response," *IEEE Transactions on Power Systems*, 2023.

[22] A. M. Quelhas, E. Gil, and J. D. McCalley, "Nodal prices in an integrated energy system," *International Journal of Critical Infrastructures*, vol. 2, no. 1, pp. 50–69, Dec. 2006.

[23] T. Jiang, H. Deng, L. Bai, R. Zhang, X. Li, and H. Chen, "Optimal energy flow and nodal energy pricing in carbon emission-embedded integrated energy systems," *CSEE Journal of Power and energy Systems*, vol. 4, no. 2, pp. 179–187, Jun. 2018.

[24] C. Wang, W. Wei, J. Wang, L. Wu, and Y. Liang, "Equilibrium of interdependent gas and electricity markets with marginal price based bilateral energy trading," *IEEE Transactions on Power Systems*, vol. 33, no. 5, pp. 4854–4867, Jan. 2018.

[25] L. Deng, Z. Li, H. Sun, Q. Guo, Y. Xu, R. Chen, J. Wang, and Y. Guo, "Generalized locational marginal pricing in a heat-and-electricity-integrated market," *IEEE Transactions on Smart Grid*, vol. 10, no. 6, pp. 6414–6425, Mar. 2019.

[26] G. Pan, W. Gu, Z. Wu, Y. Lu, and S. Lu, "Optimal design and operation of multi-energy system with load aggregator considering nodal energy prices," *Applied Energy*, vol. 239, pp. 280–295, Apr. 2019.

[27] M. Kohansal, A. Sadeghi-Mobarakeh, S. D. Manshadi, and H. Mohsenian-Rad, "Strategic convergence bidding in nodal electricity markets: Optimal bid selection and market implications," *IEEE Transactions on Power Systems*, vol. 36, no. 2, pp. 891–901, Mar. 2020.

[28] L. Zheng, J. Wang, Y. Yu, G. Li, M. Zhou, Q. Xia, and G. Xu, "On the consistency of renewable-to-hydrogen pricing," *CSEE Journal of Power and Energy Systems*, vol. 8, no. 2, pp. 392–402, Mar. 2022.

[29] X. Dou, J. Wang, D. Fan, Z. Li, X. Liang, and J. Yang, "Interaction mechanism and pricing strategy of hydrogen fueling station for hydrogen-integrated transportation and power systems," *IEEE Transactions on Industry Applications*, vol. 58, no. 2, pp. 2941–2949, Mar-Apr. 2021.

[30] I. Saedi, S. Mhanna, and P. Mancarella, "Integrated electricity and gas system modelling with hydrogen injections and gas composition tracking," *Applied Energy*, vol. 303, p. 117598, Dec. 2021.

[31] P. Zhao, C. Gu, Z. Hu, D. Xie, I. Hernando-Gil, and Y. Shen, "Distributionally robust hydrogen optimization with ensured security and multi-energy couplings," *IEEE Transactions on Power Systems*, vol. 36, no. 1, pp. 504–513, Jan. 2020.

[32] P. Zhao, X. Lu, Z. Cao, C. Gu, Q. Ai, H. Liu, Y. Bian, and S. Li, "Volt-var-pressure optimization of integrated energy systems with hydrogen injection," *IEEE Transactions on Power Systems*, vol. 36, no. 3, pp. 2403–2415, May. 2020.

[33] A. De Corato, I. Saedi, S. Riaz, and P. Mancarella, "Aggregated flexibility from multiple power-to-gas units in integrated electricity-gas-hydrogen distribution systems," *Electric Power Systems Research*, vol. 212, p. 108409, Nov. 2022.

[34] S. Wang, H. Hui, Y. Ding, and Y. Song, "Long-term reliability evaluation of integrated electricity and gas systems considering distributed hydrogen injections," *Applied Energy*, vol. 356, p. 122374, 2024.

[35] S. Wang, H. Hui, and J. Zhai, "Short-term reliability assessment of integrated power-gas systems with hydrogen injections using universal generating function," *IEEE Transactions on Industry Applications*, vol. 59, no. 5, 2023.

[36] C. Shao, Y. Ding, and J. Wang, "A low-carbon economic dispatch model incorporated with consumption-side emission penalty scheme," *Applied Energy*, vol. 238, pp. 1084–1092, Mar. 2019.

[37] H. Hui, M. Bao, Y. Ding, J. Yan, and Y. Song, "Probabilistic integrated flexible regions of multi-energy industrial parks: Conceptualization and characterization," *Applied Energy*, vol. 349, p. 121521, 2023.

[38] Several policies and measures to support the development of the hydrogen energy industry (trial). [Online]. Available: http://xxgk.jl.gov.cn/szf/ gkml/202212/t20221205_8643380.html.

[39] S. Mhanna, I. Saedi, P. Mancarella, and Z. Zhang, "Coordinated operation of electricity and gas-hydrogen systems with transient gas flow and hydrogen concentration tracking," *Electric Power Systems Research*, vol. 211, p. 108499, 2022.

[40] Gas Safety (Management) Regulations. [Online]. Available: https:// www.legislation.gov.uk/uksi/1996/551/introduction/made.

[41] M. Abeysekera, J. Wu, N. Jenkins, and M. Rees, "Steady state analysis of gas networks with distributed injection of alternative gas," *Applied Energy*, vol. 164, pp. 991–1002, 2016.

[42] M. Bus, "Review of the impact of hydrogen addition to natural gas on gas turbine combustion," Jun. 2013. [Online]. Available: http://essay.utwente.nl/69334/

[43] Github repository. [Online]. Available: https://github.com/ ShengWang-EE/J12-nodal-energy-price-H-IEGS/blob/main/ Supporting_document___v1.pdf.

[44] F. Li and R. Bo, "Dcopf-based lmp simulation: Algorithm, comparison with acopf, and sensitivity," *IEEE Transactions on Power Systems*, vol. 22, no. 4, pp. 1475–1485, 2007.

[45] S. Wang, J. Zhai, H. Hui, Y. Ding, and Y. Song, "Operational reliability of integrated energy systems considering gas flow dynamics and demand-side flexibilities," *IEEE Transactions on Industrial Informatics*, 2023.

This article has been accepted for publication in IEEE Transactions on Sustainable Energy. This is the author's version which has not been fully edited and content may change prior to final publication. Citation information: DOI 10.1109/TSTE.2024.3372628

14

[46] Y. Bo, M. Bao, B. Yang, Y. Ding, and Y. Huang, "A semi-markov stochastic model for operational reliability assessment of hybrid ac and lcc-vsc-based dc system with remote wind farms," *IEEE Transactions on Power Systems*, 2024.

[47] A. Martinez-Mares and C. R. Fuerte-Esquivel, "A unified gas and power flow analysis in natural gas and electricity coupled networks," *IEEE Transactions on Power Systems*, vol. 27, no. 4, pp. 2156–2166, Nov. 2012.

[48] S. Wang, J. Zhai, and H. Hui, "Optimal energy flow in integrated electricity and gas systems with injection of alternative gas," *IEEE Transactions on Sustainable Energy*, vol. 14, no. 3, 2023.

[49] Australian Energy Market Operator . [Online]. Available: https://www.aemo.com.au/.

[50] National Oceanic andAtmospheric Administration . [Online]. Available: https://www.noaa.gov/.

[51] A Gas Market Plan research project. [Online]. Available: https://www.nationalgas.com/document/135396/download.

[52] Energy Internet Operation and Simulation Platform. [Online]. Available: http://www.eisimu.com/page/index_main.html.

Pierluigi Siano (Senior Member) received the M.Sc. degree in electronic engineering and the Ph.D. degree in information and electrical engineering from the University of Salerno, Salerno, Italy, in 2001 and 2006, respectively. Since 2021, he has been a Distinguished Visiting Professor with the Department of Electrical and Electronic Engineering Science, University of Johannesburg, Johannesburg, South Africa. He is currently a Professor and the Scientific Director of the Smart Grids and Smart Cities Laboratory, Department of Management and Innovation Systems, University of Salerno. He has co-authored more than 370 articles published in international journals that received in Scopus more than 13,500 citations with an H-index equal to 57. His research interests include demand response, energy management, integration of distributed energy resources in smart grids, and electricity markets, and on planning and management of power systems. He was a Highly Cited Researcher in Engineering by the Web of Science Group in 2019, 2020, and 2021. He has been the Chair of the IES TC on Smart Grids. He is an Editor of the Power and Energy Society Section of IEEE ACCESS, IEEE TRANSACTIONS ON POWER SYSTEMS, IEEE TRANSACTIONS ON INDUSTRIAL INFORMATICS, IEEE TRANSACTIONS ON INDUSTRIAL ELECTRONICS, and IEEE SYSTEMS JOURNAL.

Sheng Wang (Member) received both the Ph.D. and B. Eng degrees in electrical engineering from Zhejiang University in 2021 and 2016, respectively. He was with the State Grid (Suzhou) City & Energy Research Institute in 2021. He is currently a Post-doctoral Fellow with the State Key Laboratory of Internet of Things for Smart City, University of Macau. His research interests include the optimization and reliability evaluation of low-carbon energy systems.

Hongxun Hui (Member) received the B.E. and Ph.D. degrees in electrical engineering from Zhejiang University, Hangzhou, China, in 2015 and 2020, respectively. From 2018 to 2019, he was a visiting scholar at the Advanced Research Institute at Virginia Tech, and the CURRENT Center in the University of Tennessee. He is currently a Research Assistant Professor with the State Key Laboratory of Internet of Things for Smart City, University of Macau, Macao SAR, China. His research interests include optimization and control of power systems, demand response, and Internet of Things technologies for smart energy.

Junyi Zhai (Member) received the B.S. and Ph.D. degrees in electrical engineering from North China Electricity Power University, Beijing, China, in 2014 and 2019, respectively. He was a visiting student at the University of Birmingham during 2018 and 2019. He was a senior research engineer at the State Grid (Suzhou) City & Energy Research Institute in 2019 and 2022. His research interests include mathematical optimization techniques and power system analysis and computing.